Available online at www.sciencedirect.com
SCIENCE DIRECT
Remote Sensing of Environment 102 (2006) 402–413
Remote Sensing of Environment
www.elsevier.com/locate/rse

Normalization of the directional effects in NOAA–AVHRR reflectance measurements for an improved monitoring of vegetation cycles

Cédric Bacour, François-Marie Bréon *, Fabienne Maignan

Laboratoire des Sciences du Climat et de l'Environnement, Commissariat à l'Energie Atomique, Gif-sur-Yvette, France

Received 21 December 2005; received in revised form 23 March 2006; accepted 25 March 2006

Abstract

This paper describes a correction of directional effects in AVHRR reflectance time series. The method relies on a priori directional signatures, in the red and near infrared, for various surface covers. The reflectance normalization is applied to the historical Pathfinder AVHRR Land (PAL) data set acquired between 1981 and 1999. The high frequency variability in the reflectance time series, which is interpreted as a noise due to varying observation geometry and directional effects, is reduced by a factor greater than 1.7 for most vegetated surfaces. For the analysis of the vegetation annual cycle and its inter-annual variations, we recommend the use of the Difference Vegetation Index (DVI), following a prior correction of the directional effects, instead of the commonly used NDVI. Indeed, DVI appears more robust than NDVI to noise resulting from atmospheric perturbations, which makes it a good candidate for long-term ecological surveys and climate change studies.

Keywords: NOAA–AVHRR; BRDF correction; Vegetation cycle; NDVI; DVI

1. Introduction

The data archive acquired since 1981 by the series of Advanced Very High Resolution Radiometer (AVHRR) instruments constitutes an unrivaled historical record for monitoring and understanding the response of the Earth's biosphere to climate changes (Anyamba et al., 2002; Goetz et al., 2000; Myneni et al., 1997). Quantitative monitoring of vegetation density and photosynthetic activity relies almost exclusively on the analysis of Normalized Difference Vegetation Index (NDVI) data. NDVI is the difference of the surface reflectivity between two wavelengths [in the red (R) and in the near infrared (NIR)], normalized by their sum. The differential reflectance in these bands is strongly correlated to the photosynthetic activity of vegetation canopies, because of the large spectral shifts of the leaf optical properties. In the visible, green leaves strongly absorb the solar radiation, in proportion to the chlorophyll content: in the red, more than 80% of the incoming energy is absorbed. In the near infrared however, the photosynthetic pigments are transparent and the absorption (by the dry matter) is reduced to about 10%. On the other hand, the reflectance of bare soils is only slightly larger in the near IR than in the visible. Although NDVI varies theoretically between −1 and 1, measured values range between −0.2 and 0.05 for snow, inland water bodies, deserts and exposed soils, and increase from about 0.05 to above 0.7 together with the density and greenness of vegetation (Myneni et al., 1997). One reason for the success of the NDVI for the monitoring of vegetation from spaceborne observations is the rather small sensitivity to the observation configuration, in contrast to that of the raw reflectances (Tucker, 1979).

Indeed, variations in the sun-target-sensor geometry induced by NOAA orbits and AVHRR crosstrack scanning cause a variability in the reflectance time series that has the same order of magnitude as the signal related to actual changes in vegetation. The causes for this reflectance variability with the observation geometry are twofold: i) atmospheric scattering and transmission and ii) surface reflectance anisotropy. These effects are the main reason why reflectance time series are not used per se for monitoring vegetation changes, whereas there is a need for assimilation techniques in land surface process models. The use of NDVI reflectance ratio, as compared to individual reflectance measurements, reduces the anisotropic effects from the surface because the directional signatures are

* Corresponding author.
E-mail address: Francois-Marie.Breon@cea.fr (F.-M. Bréon).

0034-4257/$ - see front matter © 2006 Elsevier Inc. All rights reserved.
doi:10.1016/j.rse.2006.03.006

similar in these wavebands. NDVI, however, remains sensitive to changes in the observation geometry because of varying atmospheric path absorption and scattering, as well as remaining surface directional effects (Myneni & Williams, 1994; Roujean & Bréon, 1995). A recent study (Los et al., 2005) concludes that NDVI can remain largely contaminated by BRDF effects, in such extent that, in some cases, its use for detection of vegetation phenology may lead to significant errors. An alternate approach for minimizing the angular variability consists in correcting the directional effects at the reflectance level (Cihlar et al., 1997; Csiszar et al., 2001; Duchemin et al., 2002; Leroy & Roujean, 1994; O'Brien et al., 2000; Shepherd & Dymond, 2000; Strugnell & Lucht, 2001). This is achieved by fitting the actual measurements with a Bidirectional Reflectance Distribution Function (BRDF) model and extrapolating them into a standard observation geometry.

The present work focuses on such reflectance normalization applied to AVHRR time series acquired between 1981 and 1999. It follows the work of Bacour and Bréon (2005) that derived simple directional models [or Bidirectional Anisotropy Standard shapEs (BASEs)] for representative land surface types of the Earth. The BASEs were defined from the analysis of POLarisation and Directionality of the Earth's Reflectance (POLDER) (Deschamps et al., 1994; Bicheron & Leroy, 2000) directional measurements and for seven biome classes (Knyazikhin et al., 1998). The resulting reduction in noise is presented for the reflectance time series in the red and near infrared. Then, the effectiveness of the Difference Vegetation Index (DVI, defined as the difference between near infrared and red reflectances) and NDVI to characterize vegetation changes are compared.

2. Reflectance normalization principles

2.1. BASE models

The correction of the angular variability relies on a bidirectional model to bring the reflectance measurements into a standard observation geometry. The study makes use of the BASE models that define standard directional shapes as a function of the geometry of observation (defined by the solar zenith θ_s, view zenith θ_v, and relative azimuth ϕ, angles):

$$\mathrm{BASE}^j(\theta_s,\theta_v,\phi) = 1 + \left.\frac{k_1}{k_0}\right|_j \cdot F_1(\theta_s,\theta_v,\phi) + \left.\frac{k_2}{k_0}\right|_j \cdot F_2(\theta_s,\theta_v,\phi)$$

The F_1 function is the geometric kernel of the RossThick–LiSparse BRDF model (Lucht et al., 2000). F_2 is the corresponding volumetric kernel modified to account for the hot spot effect within turbid media (Maignan et al., 2004), with the value of the hot spot half width parameter fixed to 1.5°. The directional parameters $\left.\frac{k_i}{k_0}\right|_j$ (i=1,2) were determined for seven biomes (j=1,…,7) representative of the major Earth's vegetation types, according to the MODIS classification map (Knyazikhin et al., 1998): (1) grasses and cereal crops, (2) shrubs, (3) broadleaf crops, (4) savannas, (5) broadleaf forests, (6) needleleaf forests, (7) deserts. The directional parameters were estimated from POLDER-1 observations in the red (670 nm) and near infrared (865 nm) over an optimal subset of the POLDER archive made of 3511 targets (6×6 km^2) selected for their thematic homogeneity (Bacour & Bréon, 2005). In order to ensure reliable parameter estimates, the directional coverage of each target was made of at least 120 observations, with view and solar zenith angles less than 60°.

The approach was based on the observation that, although the reflectance magnitude of surface targets varies, their directional signatures are relatively constant. The BASE models then allow reconstructing any target BRDF R (θ_s, θ_v, ϕ) with a single parameter $\tilde{k}_0$ to be adjusted:

$$R(\theta_s,\theta_v,\phi) = \tilde{k}_0 \cdot \mathrm{BASE}^j(\theta_s,\theta_v,\phi)$$

Thus, for a target of known vegetation type, the BRDF modeling has only one single parameter. Compared to real observations from the POLDER instrument, the fit of the one-parameter model performs almost as well as the original three-parameter model. The error of fit is in the order of 10% in the red and 5% in the near infrared, in relative units (respectively 0.011 and 0.015 in absolute).

2.2. Reflectance correction

As there is a single free parameter in the BRDF model, the determination of the parameter $\tilde{k}_0$ requires a single reflectance measurement. It can therefore be used to estimate the target reflectance in a standard observation geometry. The standard configuration is here defined as an observation at nadir with a solar zenith angle θ_s^0 of 40°. This θ_s^0 value was chosen because it roughly corresponds to the average of the illumination angles inferred from the POLDER database.

It is also an average illumination encountered in the PAL archive. The normalized reflectance is then determined from the adequate BASE type by a simple formula:

$$R(\theta_s^0,0,0) = R(\theta_s,\theta_v,\phi) \cdot \frac{\mathrm{BASE}^j(\theta_s^0,0,0)}{\mathrm{BASE}^j(\theta_s,\theta_v,\phi)}$$

Applied on individual POLDER measurements (more than 100 measurements of the same target from different observation geometries), the normalization methodology reduces the reflectance variability by a factor larger than 2. The variability reduction is larger in the NIR (865 nm band) than in the visible (670 nm band). A likely explanation is that the visible reflectances are more affected by atmospheric contribution, both in absolute and relative, than the near IR measurements, while the proposed method does not correct for such effects.

3. Data

3.1. AVHRR data set

The present work uses the Pathfinder AVHRR Land (PAL) global reflectance data set acquired daily from July 1981 to December 1999 (Smith et al., 1997). The data set includes, together with the reflectances at a spatial resolution of 8 km, the

corresponding NDVI, geometry of observation (solar zenith, relative azimuth, and scan angles), quality flags, and cloud index. The data were recorded by four different AVHRR instruments onboard NOAA 7, 9, 11, and 14, which all performed daytime measurements during the afternoon. The spatial overlap between successive orbits allows a near-daily coverage of the Earth, weather permitting, with varying view and illumination geometries. Although the orbits of these satellites are almost sun-synchronous, they suffer from uncorrected orbital drift so that the local time of observation increases with time (Gutman, 1999; Privette et al., 1995). The radiance measurements in the red (580–680 nm) and near infrared (725–1100 nm) channels were calibrated using time-dependent calibration coefficients so as to correct for post-launch instrument degradations. The measurements in the PAL data set are corrected for Rayleigh scattering and ozone absorption, but not for aerosol scattering and water vapor absorption.

Among the other radiometric products deriving from the Global Area Coverage (GAC) AVHRR archive, the daily data from the PAL archive are little used as compared for instance to the 15-day composite NDVI processed by the Global Inventory Monitoring and Modeling Studies (GIMMS) group, or the Global Vegetation Index (GVI) data set (Gutman, 1999). Beyond the extra costs in data processing involved by daily measurements, it may be explained by some processing errors in the original PAL data set (Smith et al., 1997), affecting the solar zenith angle, the reflectances in channels 1 and 2 as well as NDVI, and the cloud screening tests. The daily 8 km binary data are now corrected for these errors. The spatial resolution of POLDER (6 km) and AVHRR data – through the GAC (4 km) and PAL (8 km) data sets – are similar. Thus, the BASE directional models derived from POLDER appear well suited for the correction of directional effects in the PAL product or any other product derived from GAC observations.

3.2. Regions of interest

AVHRR PAL data are available in tiles of 125×125 pixels, each representing a region of 1000×1000 km^2. The present study focuses on four different tiles: 1004 (East of the United States area located South of the Great Lakes, centered on [37.53°N, −81.45°W]), 1906 and 1907 (corresponding the subtropical North West part of Africa encompassing Mali, Mauritania, Burkina Faso, Ivory Coast and Guinea, and respectively centered on [19.54°N, −7.03°W] and [10.55°N, −5.42°W]), and 2103 (Western Europe encompassing most of France and its eastern bordering countries [46.7°N, 6.12°E]). These tiles were chosen because they correspond to different biome types with various vegetation cycles.

For each PAL pixel, the normalization method requires the prior knowledge of the corresponding vegetation type. For this purpose, we use the MODIS 1 km biome classification product (Knyazikhin et al., 1998). 9×9 km^2 pixels from this classification centered on the PAL pixel are used. If more than 10% of the PAL pixel area is identified as water, urban or is unclassified, it is not used further. For each remaining valid pixel, the a priori BRDF is computed as the sum of the predefined BASEs weighted by the fraction of the corresponding biomes within the pixel.

3.3. Cloud screening

Since the monitoring of land surfaces from AVHRR optical channels requires clear-sky conditions, overcast and cloud contaminated pixels are eliminated. The cloud detection tests use the cloud flags of the PAL data, based on the top of atmosphere (TOA) radiance measurements in the mid and thermal infrared channels (Agbu & James, 1994). In addition, we have applied alternative cloud screening tests relying on the normalized surface reflectances. They derive from the considerations that (i) clouds are more reflective than cloud-free surfaces and that (ii) reflectance of vegetation is significantly larger in the near infrared than in the red. In addition to the screening tests already used by Wu et al. (1995), the pixels whose reflectance level in the red or near infrared exceeds a given threshold are screened out. The thresholds correspond to maximum reflectance values associated to clear sky observations during monthly periods of synthesis (Bouffiès & Bréon, 1996), at the spatial resolution of about 6×6 km^2. The 3×3 neighborhood of each pixel failing one of these tests is also flagged as cloud.

3.4. Water vapor correction

The temporal variability of the atmospheric water vapor limits accurate characterization of the biosphere from the current PAL AVHRR data, where its effects are not accounted for (O'Brien et al., 2000). Indeed, the absorption by water vapor can decrease the radiometric signal by roughly 0.7% to 4.4% in the red, and 7.7% to 25% in the near infrared (Vermote & Vermeulen, 1999), because of the overlapping between AVHRR channels and water vapor absorption bands. The water vapor transmission is determined following the method of Vermote and Vermeulen (1999), with the total column water vapor content provided by the ECMWF 40-year Re-Analysis (ERA-40) Data Archive (Uppala et al., 2005) at a 6-h time step and at $2.5° \times 2.5°$ spatial resolution. All AVHRR data shown in the following have been corrected for water vapor absorption

4. Results

4.1. Illustration of the reflectance corrections

The impact of the surface anisotropy effects and its correction are shown in Fig. 1. This near infrared reflectance image is derived from two satellite overpasses separated by about 100 min. The discontinuity on the original image (Fig. 1a where the western part is brighter than the eastern one) clearly evidences the directional effects due to the change in the observation geometry between the two orbits. The reflectance normalization as described in Section 2.2 removes this discontinuity (Fig. 1b): the reflectance values for the eastern part of the image are decreased by about 18% whereas those for the western part are increased by 22% on average.

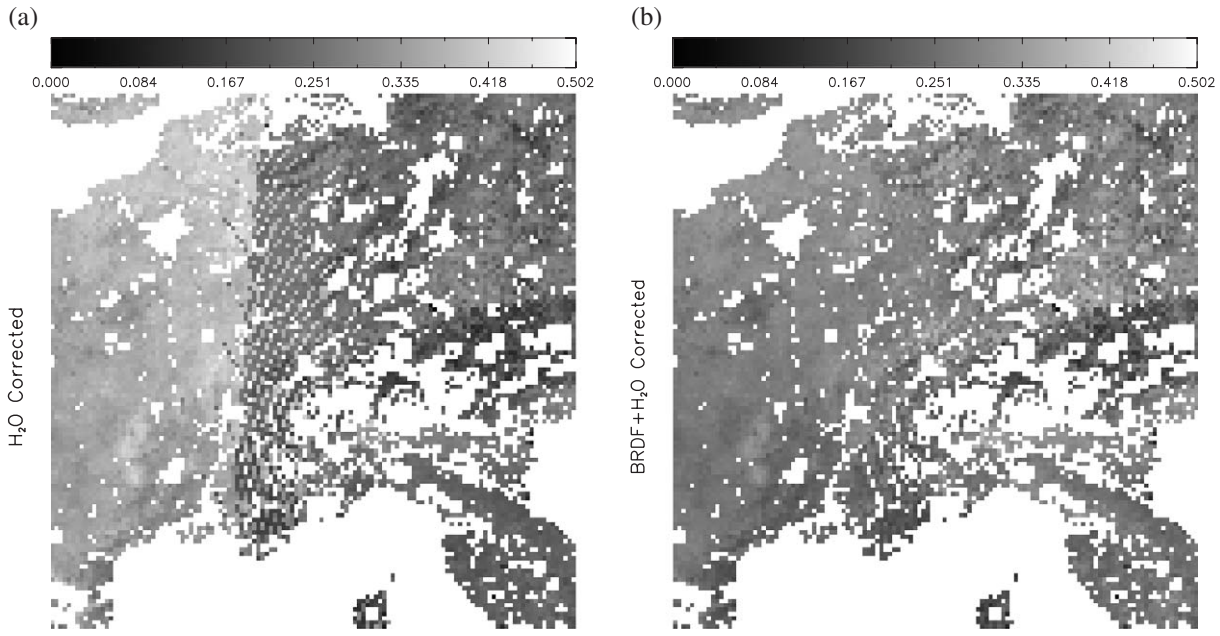

Fig. 1. Near infrared reflectance map of tile 2103 acquired on 07/23/1985 by AVHRR onboard NOAA-9, after processing of the cloud mask: (a) reflectance data only corrected for the effects of atmospheric water vapor absorption; (b) data corrected for the effects of both surface anisotropy and water vapor absorption.

Fig. 2 shows a representative time series of measured reflectances in the red and near infrared, and the corresponding NDVI and DVI, for the pixel (34.36°N, −86.63°E) (tile 1004). The lack of data during 1994 results from the failure of NOAA-11. The impact of normalization on the reflectances is particularly manifest on the inset focused on the NIR reflectances (Fig. 2b). In summer in particular, when the canopy development induces larger directional effects as compared to winter or spring where the sparseness favors more isotropic behaviours, the levels and the high frequency variability of the measurements are significantly reduced by the normalization. The results are not so striking in the visible where the atmospheric noise is larger than in the near IR, both in absolute and relative units. The benefits of normalization for DVI seem to match those previously observed in the NIR. On another hand, the short-term variability (i.e. noise) in the NDVI time series appears larger than that for DVI, after correction for the directional effects. In the following we attempt to quantify the noise in the times series for both vegetation indices.

For that purpose, the time series of reflectances and vegetation indices are fitted by the CCGVU routine (Thoning et al., 1989), specially designed to capture the seasonal cycles and inter-annual variations in temporal data (originally dedicated to CO_2 concentrations). First, the data are roughly approximated by a time dependent function $Y(t)$ combining a second-order polynomial – to represent the long-term trend – and four yearly harmonic functions – to capture the annual cycle:

$$Y(t) = \sum_{i=0}^{np=2} a_i t^i + \sum_{i=1}^{n=4} a_{2i+np-1}\sin(2\pi i t) + a_{2i+np}\cos(2\pi i t) = P_2(t) + H_4(t)$$

The residuals of the data about $Y(t)$ are then filtered twice to separate the short-term variations and the long-term trend. The filtering is performed in the frequency domain by transforming the residuals of the fit with a Fast Fourier Transform algorithm. The transformed data are then multiplied by a low pass filter function $h(f)=0.5^{(f/fc_i)^4}$ defined by the cutoff frequency fc_i. The low frequency residuals filtered at 80 days ($=1/fc_1$) are added to the harmonic functions $H_4(t)$ to determine a smooth curve tracking the short-term variations including the seasonal cycle. The long-term trend is obtained by adding the residual curve filtered at 667 days ($=1/fc_2$) to the polynomial ($P_2(t)$). These various components of the curve fitting are illustrated in Fig. 3. In the following, the smooth curve serves as a reference signal as high frequency changes in the time series are unrealistic with respect to vegetation phenology. These are therefore considered as noise. One can observe in Fig. 2 how the smooth curves remarkably captures the seasonal cycles in the temporal profiles of the reflectances and vegetation indices.

4.2. Impact of normalization on the reflectances

We now quantify the impact of the directional normalization on the noise in the time series. The noise is here defined, for each pixel, as the root mean square (RMS) of the residuals between the data (the AVHRR measurements or the corresponding BRDF corrected values) and the CCGVU fitted values. Only the pixels with more than 1000 observations available during the period of synthesis were used (this concerns 57% of the PAL pixels). Fig. 4 shows that for most pixels of the four PAL tiles analyzed (92% in the R and 99% in the NIR), the normalization leads to a reduction of the noise level. As observed on a single pixel in Fig. 2, the noise reductions are significant in the near infrared where the directional effects dominate the signal variability, while they

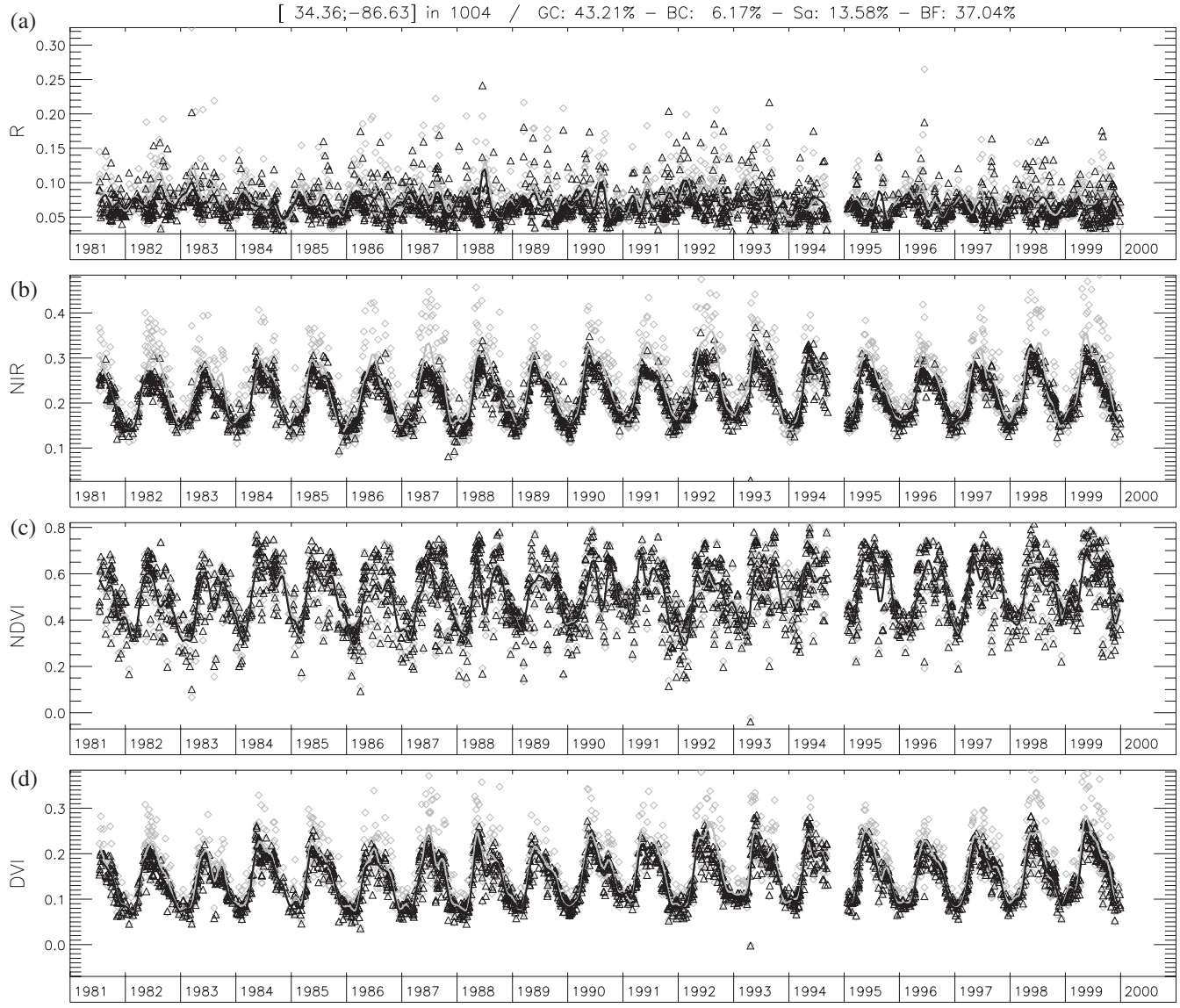

Fig. 2. Time series of the reflectances in the (a) red (R), (b) near infrared (NIR), (c) NDVI, and (d) DVI, for the pixel located at (34.36°N, −86.63°E) (tile 1004); also provided are their biome composition in grasses and cereal crops (GC), broadleaf crops (BC), savanna (Sa), broadleaf forest (BF). Grey: AVHRR data; Black: data corrected for the directional effects.

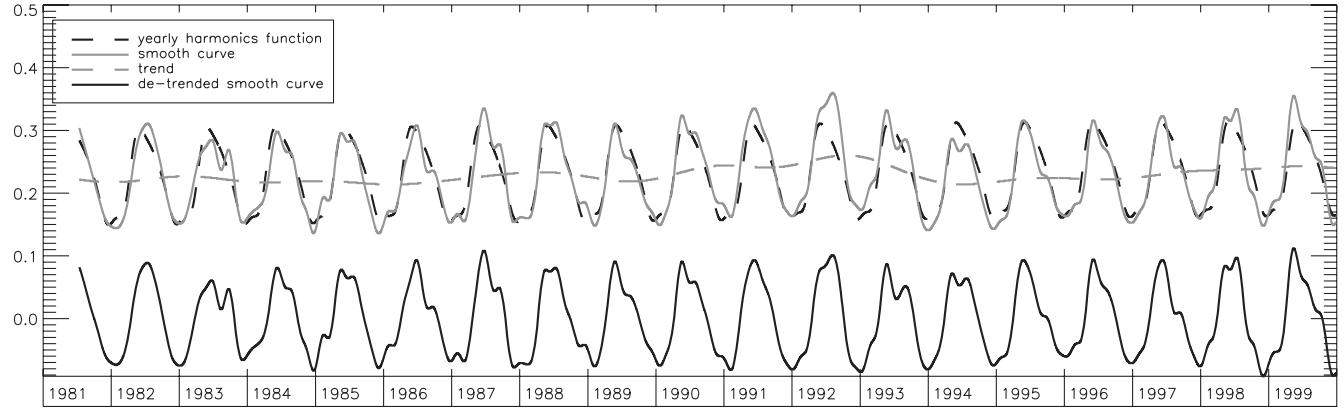

Fig. 3. Illustration of the curve fitting by the CCGVU routine on the near infrared reflectance time series for the pixel of coordinates (34.36°N, −86.63°E). Are shown the sum of the four harmonic functions that approximate the yearly oscillations (dashed line), the smooth curve (corresponding to the reference radiometric signal), the trend, and the de-trended seasonal smooth curve.

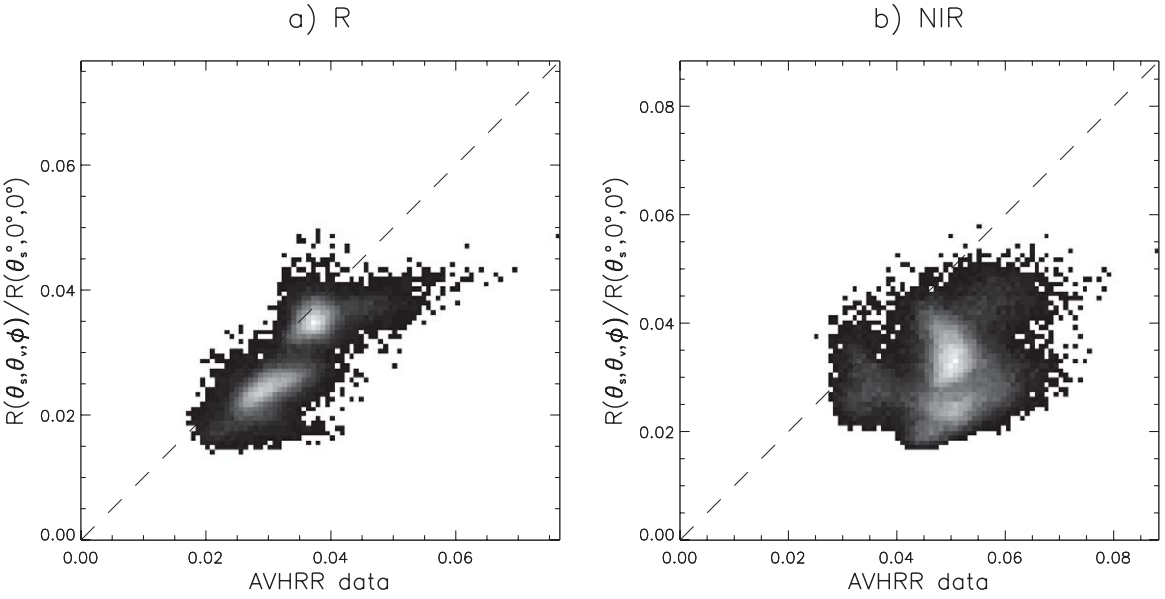

Fig. 4. Comparison of the reflectance noise between the actual AVHRR reflectance data and those corrected for the directional effects, in the (a) red and (b) near infrared and for four tiles. The noise is defined as the standard deviation of the residuals between the reflectance data and the curve fitted values. Only pixels with at least 1000 measurements during the period 1981–1999 are accounted for. Each inset is a bidimensional histogram where white color indicates the highest density of points.

are much smaller in the visible, presumably because of the dominance of atmospheric scattering noise, not corrected by the normalization procedure. On average, the noise is reduced by a factor of 1.65 in the NIR and 1.18 in the visible. There are some spatial structures in the noise reduction however. Indeed, the tiles in northern latitudes (tiles 1004 and 2103) show a noise reduction by an average factor of 1.97 and 1.25 in the NIR and R, respectively. The same ratios are only 1.40 and 1.12 for the African tiles (1907 and 1906). There are several potential explanations for this behavior: i) desert surfaces show a larger variability in their reflectance directional signatures than vegetated surface do, so that a single BASE performs poorly for this surface cover (Bacour & Bréon, 2005); ii) atmospheric aerosol, in particular desert dust, are more present over the African tiles than over the mid-latitudes tiles, which generate additional noise in the reflectance that is not corrected by the normalization procedure.

Fig. 5 details the noise reduction as a function of biome (according to MODIS classification). It shows the ratio between the noise of the original reflectance time series and that after normalization, so that a value greater than one indicates a noise reduction. The range of the ratio is significantly larger in the near infrared than in the red, with higher mean values, except for shrubs and deserts. The gains are the largest for the land surfaces where the vegetation coverage is dense, broadleaf crops and broadleaf forest in particular. The lower mean value of the ratio in the NIR for needleleaf forests can be explained by an increased contribution of the atmospheric noise in relation to the low reflectance levels usually observed for that vegetation type. The large interval of variation with a mean ratio below 1.5 for grasses and cereal crops in the NIR is due to the variability in vegetation coverage during the vegetation cycle: this translates into variations of the directional signatures not well reproduced by the corresponding BASE model. The normalization impacts are also least for sparsely vegetated surfaces (shrubs and deserts), which are more isotropic in their reflectance and are more subject to atmospheric aerosol.

4.3. Information content of NDVI and DVI

4.3.1. Signals of vegetation activity

The potentials of a given vegetation index (VI) to characterize the surface and its temporal evolution is evaluated with respect to three criteria quantifying its information content. To evaluate the useful information that can be inferred from the time series, we have defined the ratio of the signal to noise when considering i) the mean radiometric signal, ii), the seasonal signal, and iii) the inter-annual signal. They are estimated from the curve fitted data (Fig. 3). The mean signal is determined as the mean of the smooth curve over the 1981–1999 period. The seasonal signal corresponds to the standard deviation of the de-trended smooth curve. The inter-annual signal is defined as the standard deviation of the so-called "trend" defined by the CCGVU decomposition. The information content of the seasonal signal is particularly relevant for the analysis of the annual vegetation cycle, i.e. onset and length of the vegetation growing season, that greatly impact the uptake of atmospheric carbon dioxide by the biosphere (Chrukina et al., 2005). On the other hand, the signal to noise ratio based on the trend quantifies the capability to detect inter-annual variations in biomass production.

4.3.2. Information content of NDVI and DVI profiles

Fig. 6 compares the signal to noise ratios (SNRs) based on the NDVI and DVI time series for the four tiles together. In most cases, the SNRs obtained with DVI are larger than those of NDVI: for the mean signal, 76% of the pixels correspond

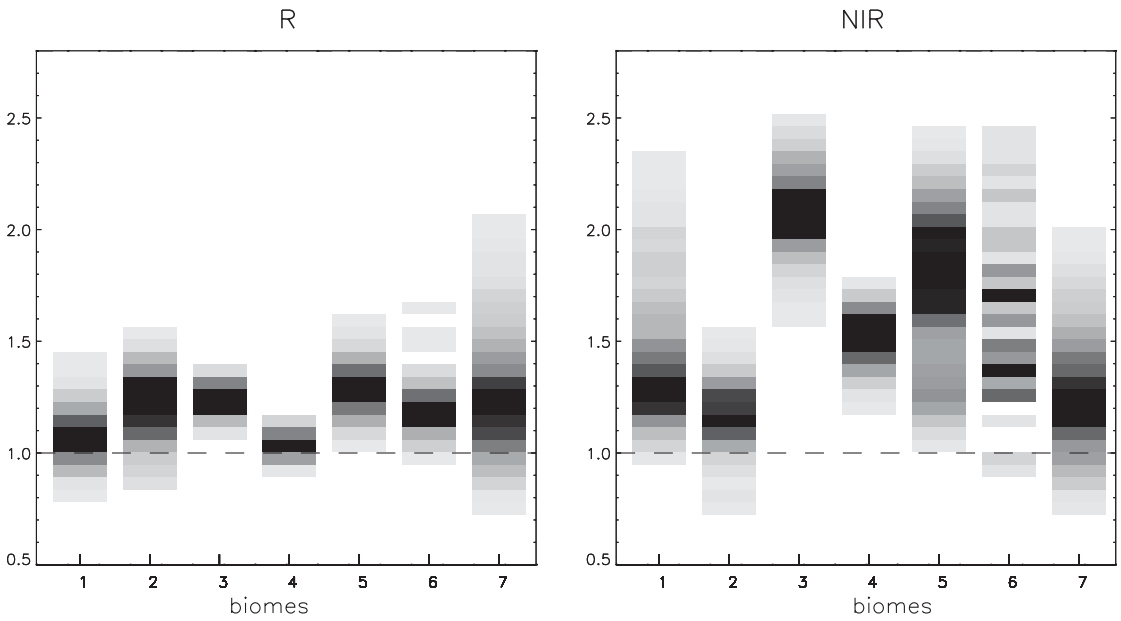

Fig. 5. Density of the ratios between the reflectance noise associated to the actual AVHRR reflectance data and those corrected from the directional effects, as a function of the biome type in the red and near infrared. The biomes considered are: (1) grasses and cereal crops (3179 pixels), (2) shrubs (698 pixels), (3) broadleaf crops (2322 pixels), (4) savannas (5981 pixels), (5) broadleaf forests (4669 pixels), (6) needleleaf forests (89 pixels), and (7) deserts (2909 pixels). Only pixels with a fractional cover greater than 70% of the same biome class and with at least 1000 measurements during the period 1981–1999 are used. Each bar corresponds to a histogram where cells darkens with the population density.

to SNR(DVI) greater than SNR(NDVI); for the seasonal signal, the proportion is of 76%; it is of 57% when considering the inter-annual trend of the signal. A large fraction of the pixels with a higher SNR(NDVI) belong to the African tile 1906. The same analysis for the three other tiles alone gives 90%, 91% and 67%, respectively. Again, the poor performance of the directional normalization for low vegetation coverage explains the differing statistics. For the tile 1906, the pixels of grass and crop biomes correspond to sparsely vegetated surfaces with short growing periods. This explains why, over the full year, these surfaces respond similarly to shrubs or deserts.

When analyzing the mean signal, the SNR is rather high for both DVI and NDVI. Indeed, both SNRs are larger than 2.5 for the whole of the pixels. The median value is 5.4 for NDVI and 6.2 for DVI. Clearly, both vegetation indices provide useful information that may be associated with photosynthetic activity. The information content of DVI appears somewhat more reliable than that inferred from NDVI. This may derive from the fact that DVI is more impacted by the near infrared for which the normalization works better, and has less noise (because of higher surface reflectance levels combined to lower atmospheric effects) than the red channel. Indeed, even if the contributions to DVI in both wavelengths are similar in absolute values, the near infrared channel has a greater impact than the red band in relative units. For NDVI, however, considering that it is a ratio of the reflectances in the two spectral bands, the R and NIR measurements have the same contribution in relative units. It is consequently more impacted by the noise of the red channel, dominated by atmospheric perturbations.

For the detection of the seasonal cycle, the average SNR is 1.5 times larger for DVI than for NDVI. This demonstrates the better capability of the DVI to describe the vegetation cycle and,

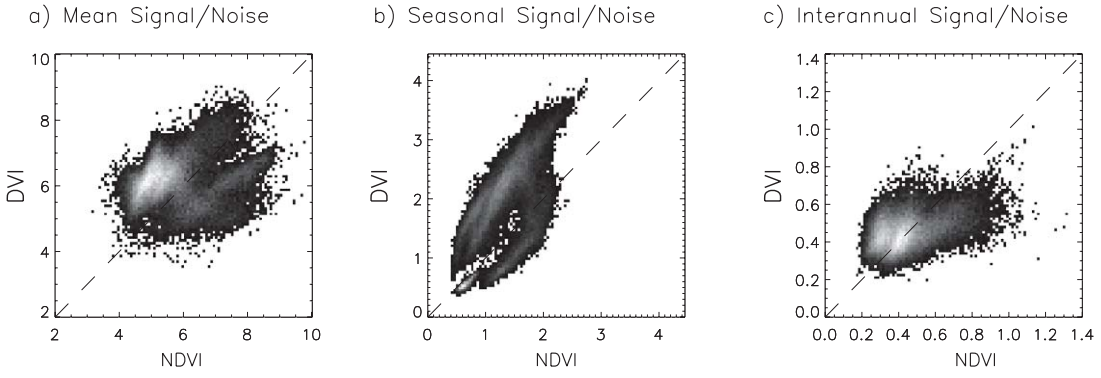

Fig. 6. Comparison of the signal to noise ratios of NDVI and DVI (after the BRDF correction) when considering (a) the mean signal, (b) the seasonal signal, and (c) the inter-annual signal. Only pixels with at least 1000 measurements during the period 1981–1999 are used.

potentially, its long-term variations as a result of climate change and/or anthropogenic activities. This result confirms the preliminary observation drawn from Fig. 2 concerning the erratic time series of NDVI in comparison to that of DVI after directional correction. The seasonal cycle amplitude (quantified by the standard deviation of the de-trended smooth curve) exceeds the noise level except for desert or very sparsely vegetated surfaces.

Clearly, the long-term variations of the reflectance are significantly lower than the amplitude of the seasonal cycle. As a consequence, the signal to noise computed from the "trend" curve is significantly smaller than those based on the mean signal or the seasonal cycle. The SNRs are less than one for both DVI and NDVI. This does not mean that a radiometric trend cannot be detected from the satellite data as many measurements are available for that purpose. Nevertheless, we stress that the estimation of the trend according to the temporal profiles of daily vegetation indices is probably biased by the confounding effect of the orbital drift. Indeed, the drift of NOAA satellite orbits leads to rather late afternoon overpasses. As a consequence, the sun zenith angles get large and may significantly exceed the validity domain of the BASEs (which is [0°, 60°] for the view and solar zenith angles) by the end of the satellite lifetime.

Fig. 7 highlights the benefits of using DVI instead of NDVI by biome type. Values of the ratio between the SNRs of NDVI and DVI less than 0 indicate that the DVI conveys more information than NDVI. As previously mentioned, the information content of DVI exceeds that of NDVI for the surfaces with the greatest vegetation cover, namely broadleaf crops, savannas, broadleaf forests, and needleleaf forests. The use of DVI appears even more relevant for studying seasonal cycles as shown by the low values of the ratio SNR(NDVI)/SNR(DVI). The poor results obtained for grasses and cereal crops and shrublands (mainly in the African tiles) are due to the sparseness of the vegetation that predominates during the vegetation cycle, thus increasing the influence of the soil background to the reflected radiance. The latter being more isotropic than simulated by the BASE model, therefore the directional correction performs poorly.

5. Towards a monitoring of vegetation phenology

The BRDF corrected time series of DVI are thus expected to permit a more reliable analysis of vegetation changes and dynamics than with the corresponding NDVI series. In particular, DVI time series can be used to estimate key phenological metrics related to the amplitude and length of the vegetation cycle. It is however necessary to question the adequacy of the a priori BASE with the "true" surface anisotropy and to evaluate the impact of normalization on the actual time course of the vegetation signal. The normalization is based on the assumptions that the directional signatures are invariant within the predefined surface cover types and temporally stable so that the BRDF of a given pixel only varies in magnitude but not in shape. Hence, seasonal variations of the surface directional signature are neglected whereas some studies indicate a variability with the vegetation cycle (Schaaf et al., 2002). Indeed, a BASE model is built to represent an average BRDF, encompassing various phenological vegetation states within a biome type.

We here examine the impact of the surface anisotropy annual cycle on some phenological indicators estimated from the time series. We focus on two phenological stages corresponding to the dates of onset and end of the vegetation growing season, as well as the magnitude of the annual signal. Because of the difficulty to confront remotely sensed estimates at AVHRR spatial resolution with corresponding phenological in situ observations, the study is based on radiative transfer simulations. The latter allow also controlling the uncertainties between the anisotropy of the scene considered and the a priori BASE. Temporal variations of the optical properties for several benchmark surfaces are simulated with the Ross-Li BRDF model, the parameters of

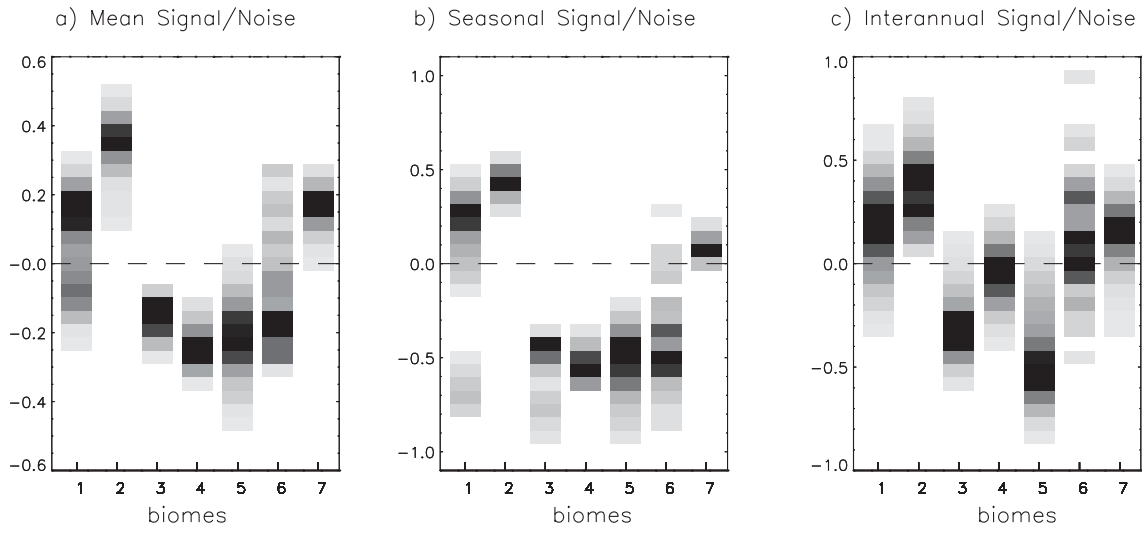

Fig. 7. Density of the logarithm of the ratios between the SNR of NDVI and DVI, as a function of the biome type when considering (a) the mean, (b) the seasonal, and (c) the inter-annual, signals.

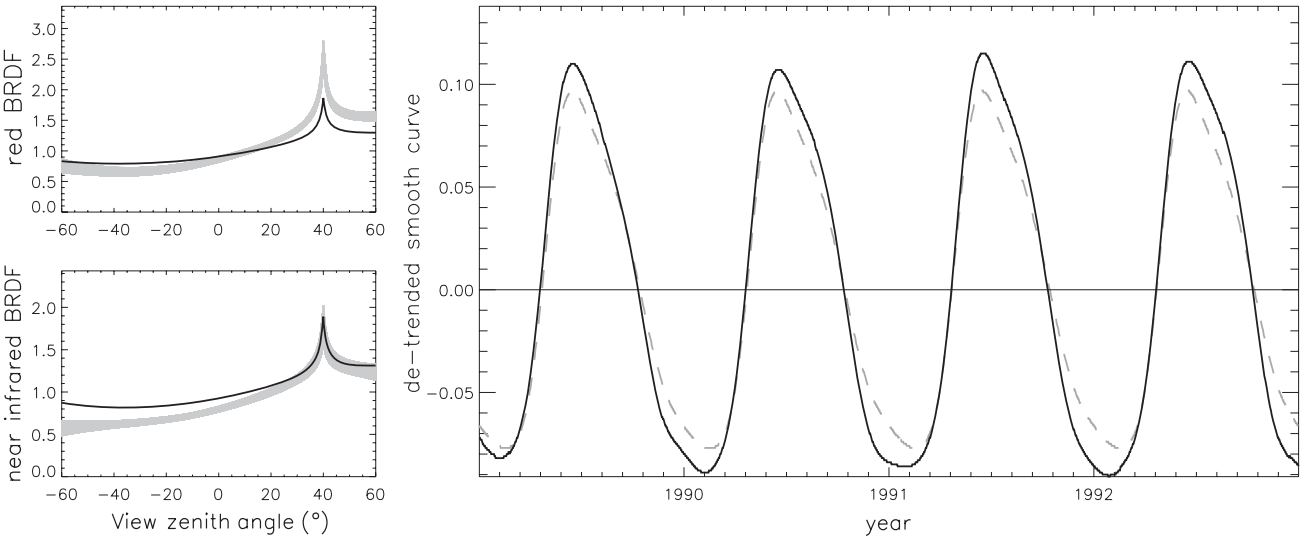

Fig. 8. Left: Envelope of the seasonal variations of the surface BRDF in the red (up) and near infrared (bottom) (derived from the broadleaf forest BASE) used to generate the reflectance time series (grey) and BASE (broadleaf crops) model used for normalization (black), as a function of the view zenith angle in the principal plane. Right: zoom on the corresponding de-trended DVI smooth curves determined from the true daily BRDFs in the standard observation geometry (grey dashed line) and from the data normalized with the prescribed BASE (black plain line).

which are varied to mimic various vegetation annual cycles. Three annual cycles of the isotropic reflectance component $\tilde{k}_0$ are simulated in the red and near infrared; they derive from true AVHRR measurements in both wavelengths for surfaces of different vegetation canopy. Temporal changes of the surface directional signature are simulated by varying the $\frac{k_i}{k_0}|_j$ directional parameters of each BASE around their nominal value, considering three annual cycles in each waveband. The latter have been estimated from POLDER-2 observations (decadal synthesis level 3 products, Lacaze, 2005) over various homogeneous surfaces, as the barycenters of the three main classes encompassing the most characteristic annual profiles. So as to account for intra-class variability, three magnitudes of these standard profiles are considered. This represents a total of 1701 different scenarios that are used to simulate the reflectance time series – in the red and in the near infrared – in the standard configuration as well as in AVHRR observation geometries. The latter are those of a pixel from the database in order to represent both realistic temporal changes of the viewing geometry and the orbital drift effect. The time series simulated in AVHRR observation geometry are then normalized by each of the BASE model, thus introducing a bias between the a priori directional shape and the "true" surface BRDF. This is illustrated in Fig. 8 (left) where the reflectances in both wavelengths are simulated using a BRDF parameterization deriving from the original broadleaf forest BASE, whereas the BASE used for normalization corresponds to that of broadleaf crops.

Finally, the DVI values are determined from the reflectance time series. The de-trended smooth curves deriving from the normalized reflectances are compared to the benchmark time series computed in the standard observation geometry. The case of Fig. 8 (right) indicates how the choice of the a priori BASE can impact the amplitude of the DVI seasonal cycle. On another hand, the onset and end dates of the cycles appear only slightly impacted. The latter are simply determined here as the dates

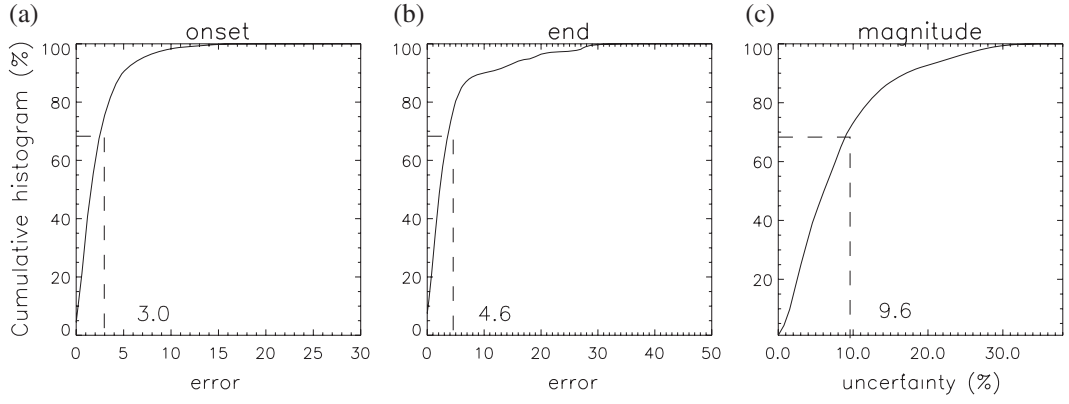

Fig. 9. Cumulative histograms of the estimation error on the (a) onset, (b) end and (c) magnitude, of the seasonal cycles. For the magnitude, the uncertainty is defined as the root mean square error between the values estimated from the signal normalized with inadequate BASEs and the true values, divided by the mean of the latter. The values of the error corresponding to one standard deviation are also indicated.

where the smooth curves intersects the *x*-axis. The global errors on the estimation of the phenological parameters are determined over all cases, as the root mean square error between the values derived from the normalized time series and those inferred from the benchmark profiles (for the signal magnitude parameter, it is expressed as an uncertainty with respect to the mean of the true values). Fig. 9 presents cumulative histograms of the estimation errors on the onset, end and magnitude, of the seasonal cycles. The determination of onsets and ends appears slightly affected by faulty constraint on the a priori knowledge of the surface anisotropy, considering the quite disadvantageous cases that were simulated. The determination error for the onset and the end of the growing season are respectively of 3 and 4.6 days (values of one standard deviation of the root mean square of the estimation errors). On the other hand, the estimation error for the magnitude of the seasonal signal is 9.6% on the average (RMS), indicating that it has to be interpreted with caution. The same analysis based on the time series of near infrared reflectances and NDVI provide less reliable phenological parameters: the error of determination for the onset and end is respectively of 3.4 and 4.8 days when using the NIR reflectances, and of 6.2 and 8.9 days when using NDVI. These results confirm that DVI provides a more reliable information for estimating vegetation phenological stages than the other radiometric signals.

6. Discussion

Despite the findings that promote the use of DVI for monitoring long-term changes in vegetation activity, especially in mid-latitudes, the corrected time series present undesirable features. In particular, DVI is still sensitive to the orbital drift effects, despite the normalization of the reflectances in the red and near infrared. This must be attributed to the violation of the domain of validity of the standard BRDF models, associated to solar zenith angles higher than 60° by the end of each satellite lifetime. Clearly, the normalization error increases together with the distance between the actual observation configuration and the standard geometry. In addition, the time series are not corrected for the aerosol scattering, including the impact of stratospheric aerosols, which is expected to increase with the sun angle. Obviously, the long time trend has to be interpreted with caution because it is very likely confounded with the inter-sensor changes and the orbital drift effect. Indeed, by construction of the fit to the time series, most of the impacts of these artifacts of vegetation change are entirely contained in the trend part of the fitted signal. When using the seasonal information (de-trended smooth curve), DVI appears superior to NDVI because it is more robust to noise, due to imperfect corrections for aerosol effects or cloud detection (Figs. 2 and 6) which has a larger relative impact on NDVI. Therefore, the de-trended seasonal cycle signal is recommended for quantitative estimation of the long-term variability of the vegetation phenology (through the analysis of the parameters related to the length of the vegetation growing season).

On another hand, contrary to NDVI, the Difference Vegetation Index cannot be used per se to accurately estimate a biophysical variable characterizing the state of vegetation. Indeed, we have investigated the possibility to relate DVI to *LAI* and/or *fAPAR* from radiative transfer model simulations. In spite of the fact that the observation geometry was fixed to the standard previously defined (viewing at nadir and sun zenith angle of 40°), the high dispersion of the points in the space defined by the joint values of DVI and of the biophysical variable of interest hinder establishing a reliable relationship between them. The dispersion increases with the vegetation cover and is larger than that obtained for NDVI.

Other studies stressing the importance of BRDF normalization for accurate estimation of vegetation phenology can be found in the paper of Los et al. (2005). They conducted a similar normalization study, however using a different methodology for deriving the BRDF models, to reduce the directional effects in AVHRR NDVI time series. Working both with radiative transfer model simulations and with 10-day PAL data, they observed a reduction of the BRDF effects in NDVI data by 50% to 85%. They concluded that the correction of the effects of the surface anisotropy is mandatory to retrieve a correct vegetation phenology from AVHRR NDVI time series. They also determined that the signal-to-noise ratio in NDVI seasonal variations is larger than in the long-term trend signal.

7. Summary and conclusion

Standard directional signatures (BASEs) have been defined from POLDER-1 observations for seven types of biome. They are used to correct the reflectance time series measured by AVHRR for the directional effects. The study makes use of the daily observations from the PAL archive acquired between 1981 and 1999, at a spatial resolution (8 km) coherent with the BASE definition (6 km). Prior to normalization, the reflectance data have been corrected for water vapor absorption and screened from clouds. The results clearly demonstrate the relevance of the approach as attested by the average reduction of the high frequency variability (interpreted as noise in the time series) by a factor 1.18 in the red channel and 1.65 in the near infrared. The improvement is particularly significant at mid-latitudes where a deep and permanent vegetation cover is observed. On the other hand, the improvement is less significant over deserts and sparsely vegetated surfaces; this is due to an increased variability in surface BRDFs that cannot be accounted for by a single BASE, and a higher impact of atmospheric aerosols.

Based on these standardized reflectance measurements, the study has investigated the robustness to noise of the NDVI and of the Difference Vegetation Index (DVI). The high-frequency variations of NDVI observed on the time series indicates a high sensitivity to atmospheric effects. In comparison, the temporal variations of the DVI appear smoother, albeit only after the directional normalization is applied. A few quantitative criteria confirm that DVI is less noisy than NDVI, presumably because of a lesser sensitivity to atmospheric effects mostly affecting the shorter wavelengths. This is particularly true for land surfaces with higher vegetation coverage where the reflectance

normalization is the more reliable. In this case, the use of the de-trended DVI signal is particularly relevant for monitoring inter-annual variability in vegetation phenology, based on the fluctuations of the vegetation greening and senescence dates and length of the vegetation cycle.

However, the orbital drifts effects on the reflectance are not fully corrected by our approach, in particular during the recent parts of the satellite lifetimes, when the sun zenith angle at the time of observation exceeds the BASE validity domain. As a consequence, one cannot fully trust an inter-annual variability in the amplitude of the seasonal cycle. On the other hand, the relatively smooth temporal profiles of DVI permit a more accurate determination of the vegetation greening and senescence compared to NDVI. These features of the AVHRR DVI time series should improve our knowledge on the response of the biosphere to climate changes. Our next objective will therefore be to infer these phenological stages from the corrected time series. Another improvement is expected with the use of BRDF data from the PARASOL satellite (CNES), very similar to POLDER, although with an extended directional coverage.

Acknowledgements

The NOAA/AVHRR data on which the study relies are made available by NASA at ftp://disc1.gsfc.nasa.gov/data/avhrr/. The POLDER database used for the determination of the biome specific BRDF models has been generated by Medias France and Noveltis from the measurements acquired by the CNES/POLDER-1 instrument onboard the NASDA/ADEOS-1 platform. ECMWF ERA-40 data have been obtained from the ECMWF data server. The authors also thank the reviewers for their constructive comments and corrections.

References

Agbu, P. A., & James, M. E. (1994). *The NOAA/NASA Pathfinder AVHRR Land Data Set User's Manual, Goddard Distributed Active Archive Center, NASA.* Greenbelt: Goddard Space Flight Center, 104 pp.

Anyamba, A., Tucker, C. J., & Mahoney, R. (2002). From El Niño to La Nina: Vegetation response patterns over East and Southern Africa during the 1997–2000 period. *Journal of Climate*, *15*(21), 3096–3103.

Bacour, C., & Bréon, F. -M. (2005). Variability of biome reflectance directional signatures as seen by POLDER. *Remote Sensing of Environment*, *98*, 80–95.

Bicheron, P., & Leroy, M. (2000). Bidirectional reflectance distribution function signatures of major biomes observed from space. *Journal of Geophysical Research*, *105*(21), 26669–26681.

Bouffiès, S., & Bréon, F. -M. (1996). A multi-year composite of GVI data as a clear reflectance database. *International Journal of Remote Sensing*, *17*(9), 1711–1726.

Chrukina, G., Schimel, D., Braswell, B. H., & Xiao, X. (2005). Spatial analysis of growing season length control over net ecosystem exchange. *Global Change Biology*, *11*, 1777–1787.

Cihlar, J., Ly, H., Li, Z., Chen, J., Pokrant, H., & Huang, F. (1997). Multitemporal, multichannel AVHRR data sets for land biosphere studies – artifacts and corrections. *Remote Sensing of Environment*, *60*, 35–57.

Csiszar, I., Gutman, G., Romanov, P., Leroy, M., & Hautecoeur, O. (2001). Using ADEOS/POLDER data to reduce angular variability of NOAA/AVHRR reflectances. *Remote Sensing of Environment*, *76*(3), 399–409.

Deschamps, P. -Y., Bréon, F. -M., Leroy, M., Podaire, A., Bricaud, A., Buriez, J. -C., et al. (1994). The POLDER Mission: Instrument characteristics and scientific objectives. *IEEE Transactions on Geoscience and Remote Sensing*, *2*(3), 598–615.

Duchemin, B., Berthelot, B., Dedieu, G., Leroy, M., & Maisongrande, P. (2002). Normalisation of directional effects in 10-day global syntheses derived from VEGETATION/SPOT: I. Investigation of concepts based on simulations. *Remote Sensing of Environment*, *81*, 90–100.

Goetz, S. J., Prince, S. D., Small, J., & Gleason, A. C. R. (2000). Inter-annual variability of global terrestrial primary production: Results of a model driven with satellite observations. *Journal of Geophysical Research*, *105*(D15), 20077–20091.

Gutman, G. G. (1999). On the use of long-term global data of land reflectances and vegetation indices derived from the advanced very high resolution radiometer. *Journal of Geophysical Research*, *104*(D6), 6241–6255.

Knyazikhin, Y., Martonchik, J. V., Myneni, R. B., Diner, D. J., & Running, S. W. (1998). Synergistic algorithm for estimating vegetation canopy leaf area index and fraction of absorbed photosynthetically active radiation from MODIS and MISR data. *Journal of Geophysical Research*, *103*, 32257–32276.

Lacaze, R. (2005). POLDER-2 land surface level-3 products – User manual algorithm description and product validation. http://smsc.cnes.fr/POLDER/SCIEPROD/P2-TE3-UserManual-I1.40.pdf, 71 pp.

Leroy, M., & Roujean, J. -L. (1994). Sun and view angle corrections on reflectances derived from NOAA/AVHRR data. *IEEE Transactions on Geoscience and Remote Sensing*, *32*, 684–697.

Los, S. O., North, P. R. J., Grey, W. M. F., & Barnsley, M. J. (2005). A method to convert AVHRR Normalized Difference Vegetation Index time series to a standard viewing and illumination geometry. *Remote Sensing of Environment*, *99*, 400–411.

Lucht, W., Schaaf, C. B., & Strahler, A. H. (2000). An algorithm for the retrieval of albedo from space using semiempirical BRDF models. *IEEE Transactions on Geoscience and Remote Sensing*, *38*, 977–998.

Maignan, F., Bréon, F. -M., & Lacaze, R. (2004). Bidirectional reflectance of Earth targets: Evaluation of analytical models using a large set of spaceborne measurements with emphasis on the hot spot. *Remote Sensing of Environment*, *90*, 210–220.

Myneni, R., & Williams, D. L. (1994). On the relationship between FAPAR and NDVI. *Remote Sensing of Environment*, *49*, 200–211.

Myneni, R. B., Keeling, C. D., Tucker, C. J., Asrar, G., & Nemani, R. R. (1997). Increased plant growth in the northern high latitudes from 1981 to 1991. *Nature*, *386*, 698–702.

O'Brien, D. M., Dilley, A. C., & Edwards, E. (2000). Interaction between surface and atmosphere in AVHRR shortwave channels. *10th Australasian Remote Sensing and Photogrammetry Conference, 21–25 August, Adelaide (Australia)*, 11pp.

Privette, J. L., Fowler, C., Wick, G. A., Baldwin, D., & Emery, W. J. (1995). Effects on orbital drift on advanced very high resolution radiometer products: Normalized difference vegetation index and sea surface temperature. *Remote Sensing of Environment*, *53*, 164–171.

Roujean, J. -L., & Bréon, F. -M. (1995). Estimating PAR absorbed by vegetation from bidirectional reflectance measurements. *Remote Sensing of Environment*, *51*, 375–384.

Schaaf, C. B., Gao, F., Strahler, A. H., Lucht, W., Li, X., Tsang, T., et al. (2002). First operational BRDF, albedo nadir reflectance products from MODIS. *Remote Sensing of Environment*, *83*, 135–148.

Shepherd, J. D., & Dymond, J. R. (2000). BRDF correction of vegetation in AVHRR imagery. *Remote Sensing of Environment*, *74*, 397–408.

Smith, P. M., Kalluri, S. N. V., Prince, S. D., & DeFries, R. (1997). The NOAA/NASA Pathfinder AVHRR 8-km Land Data Set. *Photogrammetric Engineering and Remote Sensing*, *63*(1), 37–31.

Strugnell, N. C., & Lucht, W. (2001). An algorithm to infer continental-scale albedo from AVHRR data, land cover class, and field observations of typical BRDFs. *Journal of Climate*, *14*, 1360–1376.

Thoning, K. W., Tans, P. P., & Komhyr, W. D. (1989). Atmospheric carbon dioxide at Mauna Loa Observatory: 2. Analysis of the NOAA GMCC data, 1974–85. *Journal of Geophysical Research*, *94*(D6), 8549–8565.

Tucker, C. J. (1979). Red and photographic infrared linear combinations for monitoring vegetation. *Remote Sensing of the Environment*, *8*, 127–150.

Uppala, S. M., Ållberg, P. W. K., Simmons, A. J., Andrae, U., da Costa Bechtold, V., Fiorino, M., Gibson, J., et al. (2005). The ERA-40 reanalysis. *Quarterly Journal of the Royal Meteorological Society* (in revision).

Vermote, E. F., & Vermeulen, A. (1999). Atmospheric correction algorithm: Spectral reflectances (MOD09)—Algorithm Technical Background Document. http://eospso.gsfc.nasa.gov/ftp_ATBD/REVIEW/MODIS/ATBD-MOD-08/atbd-mod-08.pdf, 107 pp.

Wu, A., Li, Z., & Cihlar, J. (1995). Effects of land cover type and greenness on advanced very high resolution radiometer bidirectional reflectances: Analysis and removal. *Journal of Geophysical Research*, *100*(5D), 9179–9192.